J. Res. Inst. Catalysis, Hokkaido Univ., Vol. 30, No. 3, pp. 137 to 154 (1982)

ELECTROCATALYSTS ON THE BASIS OF NICKEL AND ITS ALLOYS IN ELECTROCHEMICAL ENERGETICS SYSTEMS*

By

A. G. PSHENICHNIKOV**)

(Received November 25, 1982)

Abstract

Nickel electrocatalysts are finding ever increasing use in electrochemical energy conversion systems. The nickel surface coverage with hydrogen θ_H and with oxygen θ_0 as a function of potential has been determined at $E=0$ V (R. H. E.) $\theta_H \sim 1$, $\theta_0 \simeq 0$, at $E=0.2$ V $\theta_H \sim 0$, $\theta_0 \sim 0.1$, at $E=0.5$ V $\theta_0 \sim 1$ ($Ni(OH)_2$ monolayer). Electrolysis processes (hydrogen and oxygen evolution) on gauze electrodes with a surface layer of dispersed nickel catalyst have been investigated. In 7 N KOH at $i=0.4$ A/cm^2 and 70°C the polarizations at the electrodes amounts to 1, 6 V. An electrolyzer with an asbestos membrane operated at the same conditions in a stable manner for 20,000 hours at V=1.9 V. Electrodes on the base of $LaNi_5$ have been investigated. At $t=20$°C the capacity of an anode corresponds to the stoichiometric formula $LaNi_5H_6$. It has been shown that the exchange current of the electrochemical oxidation of absorbed hydrogen $i_0 \sim 10^{-5}$ A/cm^2) exceeds by an order of magnitude that of the hydrogen reaction at nickel.

Nickel catalysts are finding ever increasing use in electrochemical energy conversion systems: chemical power sources and electrolyzers. With respect to the activity in hydrogen reaction in alkaline electrolytes nickel and its alloys take the second place after platinum metals.

The properties of metals (adsorption and catalytic activity) at the metal/gas phase and metal/electrolyte interfaces differ substantially. Therefore as a rule the results of the studies on the surface state of metals in contact with vacuum and gas phase cannot be used to explain the processes occurring at the electrode/electrolyte interface.

In the case of platinum metals the electrochemical pulse methods give sufficiently complete information about the electrode surface state depending on metal type, surface pretreatment, presence of adsorbed substances, *etc.*[1],

*) The present paper was presented at the 5th JAPAN-USSR Seminar on Electrochemistry held in Sapporo, Sept. 16~18, 1982.

**) Institute of Electrochemistry, Academy of Sciences of the USSR, Moscow, USSR.

curves of clearly defined hydrogen and oxygen adsorption regions and a practical independence of the shape and integral characteristics of the hydrogen region of the charging curves on speed of their scanning (potential sweep in potentiodynamic curves and current density in galvanostatic curves)

Use of electrochemical methods for investigation of the state of a nickel electrode surface proves to be a more complicated task due to overlapping of the hydrogen and oxygen adsorption regions, slowness of the electrochemical hydrogen and oxygen adsorption and desorption processes and hydrogen solubility in metal bulk during cathodic polarization. For standardization of the nickel electrode surface we proposed a three-step pretreatment[2] : at $E=$ 0.2 V (against a reversible hydrogen electrode) the electrode surface is reduced. Simultaneously hydrogen is dissolved in nickel. At $E=0.1 \div 0.2$ V dissolved hydrogen is removed from nickel. Expose of the electrode at $\leqslant 0.2$ V does not result in oxidation of its surface. Then the electrode is maintained at the required potential in the range $0 \leqslant E \leqslant 0.2$ V. After pretreatment the electrode bulk is free of dissolved hydrogen and there is no adsorbed oxygen on its surface. Cathodic reduction of air-oxidized surface is effective only in the case of compact and coarse-grained nickel. The oxidized surface of highly dispersed nickel (such as skeleton nickel) cannot be reduced electrochemically.

The potentiodynamic charging curve of a nickel electrode with standardized surface is shown on Fig. 1 (curve 2). For comparison the charging curve of Pt electrode is given on the same Figure (curve 1). The capacity C at the potential E is determined by the relation :

$$C = i/W \qquad (1)$$

where i is the current density, W is the potential sweep rate. It is known that at $W<1$ V/sec $C_{Pt} \neq f(W)$, at the same time C_{Ni} depends strongly on W (Fig. 2).[2] Unlike a Pt electrode, exposure of a Ni electrode at cathodic potentials followed by a potential change to $E=0$ V leads to significant increase of differential and integral pseude capacity (Fig. 3) due to hydrogen dissolution in metal bulk. We showed that the capacity increase (the current i on Fig. 3) is not connected with oxidation of incorporated alkali metal. Fig. 4 shows the dependences of the amount of electricity in the range $E=0 \sim 0.2$ V at $W=3.7$ mV/sec after exposure at $E=-0.1$ V on the cation type and KOH solution concentration.[3] As can be seen from the figure on which potentials are referred to a hydrogen electrode in the same solution, this amount of electricity depends only on E_C and does not depend on the cation type and electrolyte concentration. The obtained data point to the

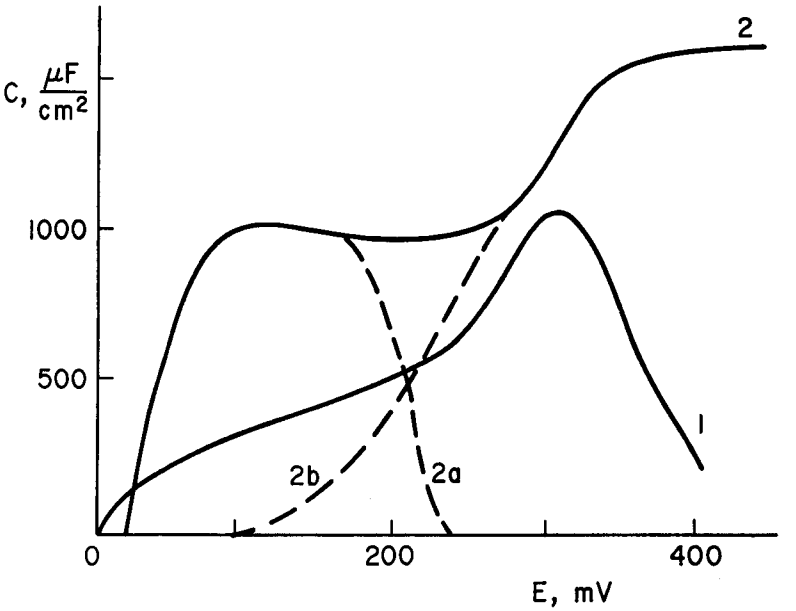

Fig. 1. Potentiodynamic C, E curves in alkaline electrolyte. 1- Pt, 2- Ni, 2a- hydrogen region, 2b- oxygen region

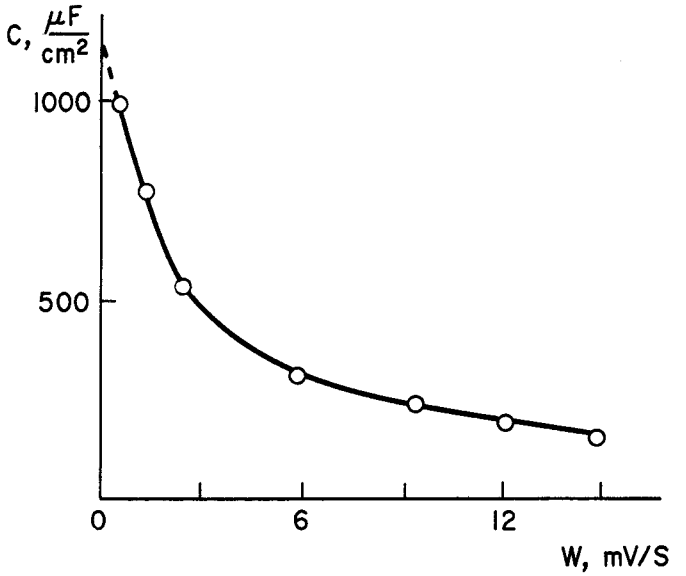

Fig. 2. A C, W-curve for nickel. Alkaline electrolyte.

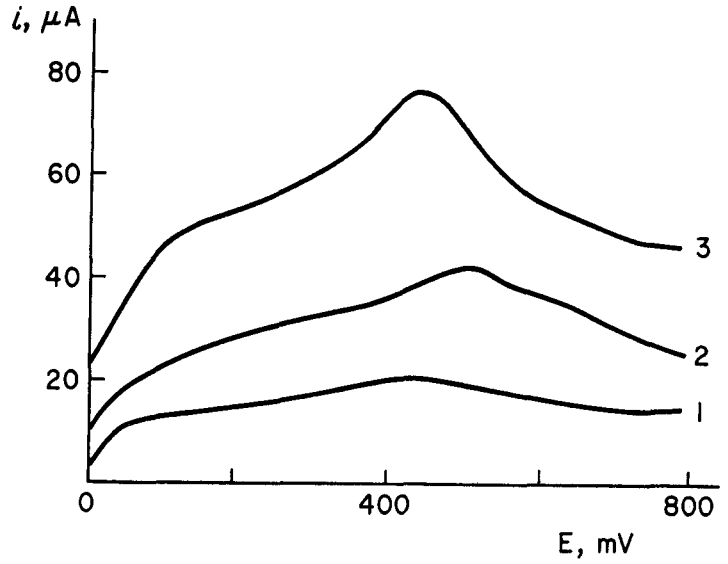

Fig. 3. *i*, *E*-curves after electrode exposure at cathodic potentials. E_c V: 1—0,0, 2— −0,1, 3— −0,2

"hydrogen" nature of the capacity on Fig. 3.

Taking into account the above data, one can assume that at equilibrium conditions at $E \geqslant 0$ ($P_{H_2} \leqslant 1$ atm) hydrogen is not dissolved in nickel.

In the potential range $0 \leqslant E \leqslant 0.5$ V the nickel electrode surface state after pretreatment is determined by the quasiequilibrium reactions:

$$H_{ads} + OH^- \rightarrow H_2O + e \qquad (2)$$

$$Ni + xOH^- \rightarrow (OH)_x^- + xe \qquad (3)$$

The reaction of nickel passing into solution

$$Ni \rightarrow Ni^+ + e \qquad (4)$$

can be neglected since the steady state rate of reaction (4) in the potential range studied was at least by two orders of magnitude lower than the rates of reactions (2) and (3).

Due to overlapping of the hydrogen and oxygen adsorption regions on nickel, their adsorption isotherms can be obtained by an independent method by means of which it is possible to determine the adsorption of one of adsorbate components. As such method we used the vacuum-electrochemical method allowing separate measurement of hydrogen adsorption on dispersed nickel[4] and the ellipsometric method by means of which we determined

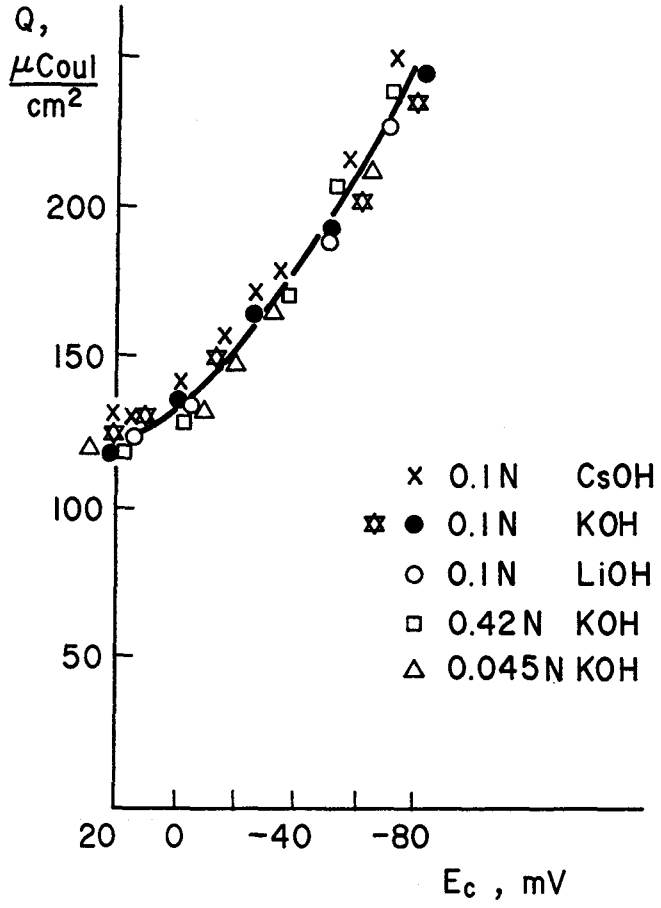

Fig. 4. Q, E_c dependences for alkaline electrolytes with different cations and for different KOH concentrations, $W=3$, 7 V/sec.

oxygen adsorption on compact nickel.[5] The results of these measurements are given on Fig. 5. To obtain the adsorption isotherm and kinetic dependences it is necessary to know the true surface value of nickel S. S is determined form the pseudocapacity of the hydrogen region of the quasiequilibrium charging curve. By comparing the pseudocapacity of the hydrogen region with the surface determined by the BET method we found the mean integral pseudocapacity of the hydrogen region per unit true surface $\bar{C}_S$, which proved to be 1120 μF/cm². The electrode surface is determined by the formula

$$S=\bar{C}/\bar{C}_S \qquad (5)$$

where $\bar{C}$ is the pseudocapacity of the hydrogen region. The quasiequilibrium

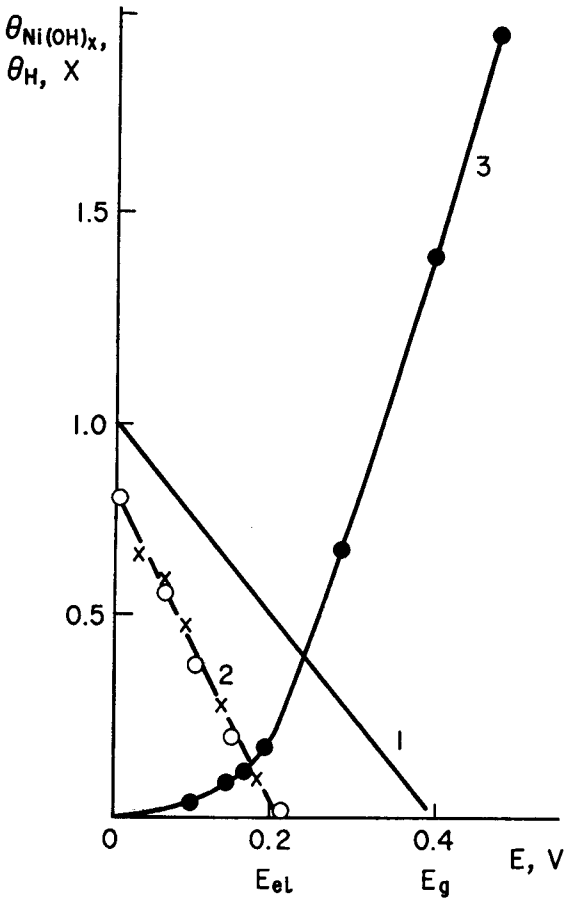

Fig. 5. Hydrogen and oxygen adsorption isotherms.
H_2 adsorption isotherm; 1-gas phase, $f=14$, 2-electrolyte, $f=7$, 3- oxygen adsorption isotherm $\theta_{OH}=1$ at $x=1$

nature of the curve is achieved provided scanning time of charging curve within the potential range $0 \leqslant E \leqslant 0.2$ V is 15~20 min. This time corresponds to $i \simeq 0.2 \times 10^{-6}$ A/cm^2 for the galvanostatic charging curve and $W \sim 0.2 \times 10^{-3}$ V/sec for the potentiodynamic charging curve. The following conclusions can be drawn from the data on Fig. 5. The inhomogeneity factor f upon contact of nickel catalyst with the gas phase is close to 15, i. e. equal to that of platinum. When an electrode was immersed into electrolyte, f_{Pt} did not change and f_{Ni} decreased approximately twice. This change can be explained by the dependence of the dipole orientation or the dipole moment value of adsorbate (hydrogen atoms, water molecules) on potential (surface

coverage by hydrogen). The hydrogen adsorption isotherm at the electrode/electrolyte interface was plotted from the data for nickel of different nature (compact nickel, carbanil nickel with small specific surface, highly dispersed skeleton nickel). Sufficiently good agreement of the results for all nickel specimens points to the similarity of the differential properties of nickel of different nature with respect to the hydrogen adsorption process. The integral properties (bond energy Me-H at $E=0$) however can differ.

By means of the data on Fig. 5 it is possible to separate the hydrogen and oxygen regions on the C, E curve (Fig. 1, dashed lines). Dependence of the surface coverage by hydrogen θ_H and by oxygen θ_0 on potential is of importance. In calculating the surface coverages it was assumed that per 1 cm^2 nickel surface there are 1.4×10^{15} Ni atoms, *i. e.*, a monolayer coverage of the surface with atomic hydrogen corresponds to 240 μcoul/cm^2, monolayer coverage with stoichiometric oxide $Ni(OH)_2$ corresponds to 480 μcoul/cm^2. It follows from Fig. 5 that at $E=0$, $\theta_H\sim0.85\div0.90$, $\theta_0\sim0$, at $E=0.2$ V $\theta_H\sim0$, $\theta_0\sim0.1$, at $E=0.5$ V, $\theta_0\sim1$. If θ_H is known it is possible to obtain information about the hydrogen reaction mechanism. In this communication we shall consider the mechanism of cathodic hydrogen evolution on skeleton nickel catalyst Ni_{Re}. The catalyst activity is determined by its specific surface $S_g=S/g$, where g is the catalyst weight in grams, and by the activity of unit surface (the exchange current of the hydrogen reaction i_o), i_o may depend on the reaction mechanism, which in its turn depends on θ_H. The exchange current is determined by extrapolation of the Tafel plots in regions of the polarization curves to their intersection with the abscis axis (logarithms of the current) and from the slope $(\partial i/\partial\eta)_{\eta\to0}$. The exchange current depends on the electrode material, electrolyte concentration and composition and temperature. More detailed studies show that in the number of cases i_o depends on S_g, on the oxidation state of the electrode surface, on promoter additions and on other catalyst properties. The results of the studies on the dependence of the exchange current i_o on electrolyte concentration (potassium hydroxide) and catalyst dispersion are given on Fig. 6 and 7. The curve of the dependence of i_o on C_{KOH} (Fig. 6) passes through a maximum at $C_{KOH}\sim$ 0.1 N. Decrease of i_o with increasing S_g (Fig. 7) can be explained by increase of the Me-H bond energy with increasing particle size (microroughness) due to nonsaturation of the bonds of nickel surface atoms.[6] The total exchange current of catalyst I_o is equal to the product $i_o\times S$. As can be seen from Fig. 8, in a wide potential range I_0 slightly depends on S.

To study the kinetics of hydrogen evolution it is necessary to perform measurements under conditions of equal accessibility of catalyst surface. Fig.

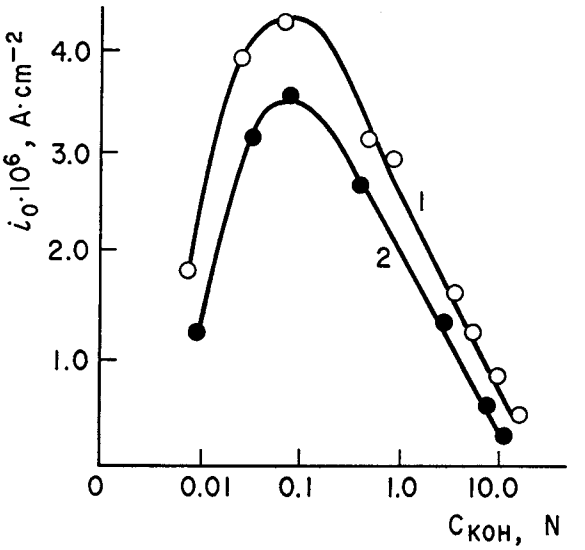

Fig. 6. Dependence of exchange current on KOH concentration, 20°C.
1-Ni_{carb} 2-Ni_{skelet}

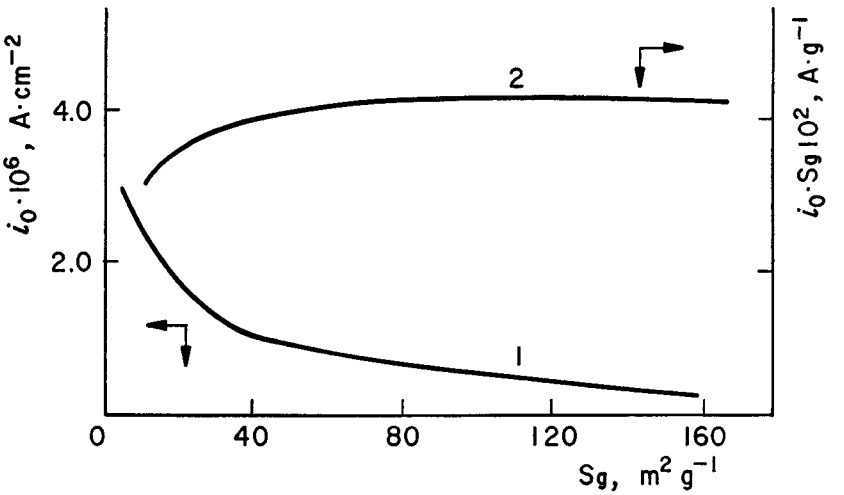

Fig. 7. Dependence of exchange current on specific surface.
1- $i_0(S_g)$ 2- $I_0 = i_0 \cdot S_g = f(S_g)$

8 shows the dependence of the current density at $E=0.12$ V (7 N KOH, 70°C) on catalyst surface per 1 cm² electrode surface S_e. S_e was increased by increasing catalyst amount (active layer thickness). It follows from Fig. 8 that the dependence i, S_e is linear, *i. e.* the catalyst surface is equally

accessible even when the electrodes work under most rigorous conditions ($E_{max}\sim 0.12$ V). The tafel plots have two parts. The experimental kinetic parameters of the hydrogen evolution process are given on Table 1.
The exchange currents i_o^a and i_o^b were determined as half the current cut off on the abscissa axis at $E=0$ by extrapolation of the 1-st and 2-nd Tafel regions respectively (see below).

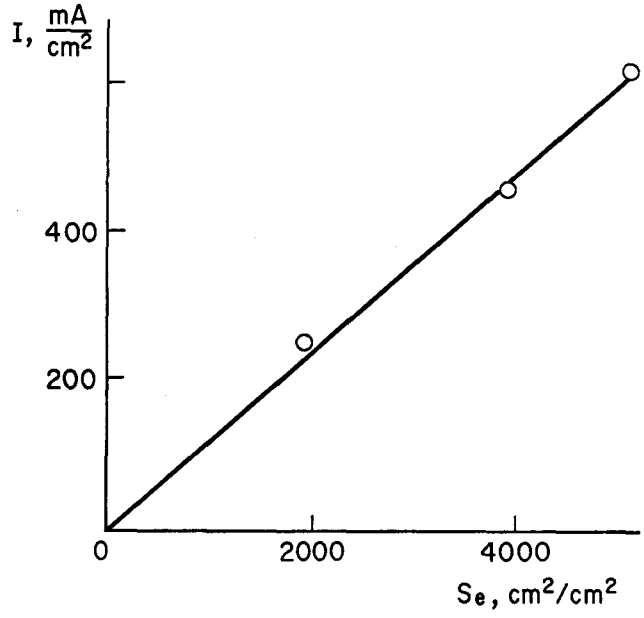

Fig. 8. Dependence of electrode current density on intrinsic layer catalyst surface, S_e. (layer thickness), 7 N KOH, 70°C.

TABLE 1. Kinetic parameters of the hydrogen evolution process on electrodes with surface skeleton catalyst

Parameters	Initial linear part of polarization curve	First Tafel region (low polarization values)		Second Tafel region (high polarization values)	
Conditions	Exchange current $\left(i_o=\frac{RT}{F}\left(\frac{\partial i}{\partial E}\right)_{E=0}\cdot 10^6\right)$ A/cm²	Dimensionless slope, B $\left(\frac{\partial E}{\partial \ln i}\right)/\left(\frac{RT}{F}\right)$	Exchange current $i_o^a\cdot 10^6$ A·cm^{-2}	Dimensionless slope, B $\left(\frac{\partial E}{\partial \ln i}\right)/\left(\frac{RT}{F}\right)$	Exchange current $i_o^b\cdot 10^6$ A·cm^{-2}
0.1 N KOH 20°C	0.6	2/3	—	2	—
7 N KON 20°C	0.04	2/3	0.06	2	0.37
7 N KOH 70°C	2.2	2/3	0.25	2	2.5

According to the data given earlier, at $E=0$, $\theta_H \sim 0.8 \div 0.9$ (Fig. 5). It can be assumed that at $E < -0.02$ V, $\theta_H \sim 1$. Under given conditions the most likely path of the hydrogen evolution reaction includes the electrochemical desorption step

$$\begin{aligned} &H_2O + e^- \rightarrow H_{ads} + OH^- \qquad (a) \\ &H_{ads} + H_2O + e^- \rightarrow H_2 + OH^- \qquad (b) \end{aligned} \tag{6}$$

If the transfer coefficients of the steps (6 a) and (6 b) are the same and $\theta_H \sim 1$, the expression for the polarization characteristic[7] assumes the form:

$$I = \frac{2\, i_o^a \left[1 - e^{(2F/RT)E}\right] \cdot e^{\frac{(1-\alpha)E}{RT}}}{i_o^a / i_o^b + e^{(F/RT)E}} \tag{7}$$

where i_o^a and i_o^b are the exchange currents of the reactions (6 a) and (6 b). At high cathodic polarization values $e^{(2F/RT)E} \ll 1$ and $e^{(F/RT)E} \ll i_o^a / i_o^b$ *i. e.*

$$I_{E \ll 0} = 2\, i_o^b \cdot e^{\frac{-(1-\alpha)F}{RT}E} \tag{8}$$

At not too negative values of E, but at $E < -0.025$ V and provided $i_o^a \ll i_o^b$ it can be assumed that $e^{(2-\alpha)E} \ll 1$ and $e^{(F/RT)E} > i_o^a / i_o^b$. In this case equation (7) assumed the form:

$$I_{E<0} = 2\, i_o^a \cdot e^{\frac{-(2-\alpha)F}{RT}E} \tag{9}$$

The dimensionless Tafel slopes in equations (8) and (9) correspond to the experimental values (Table 1) for the 2-nd (eq. 8) and 1-st (eq. 9) regions of the polarization curves on Fig. 9. Thus in the 1-st and 2-nd parts the slow steps are the discharge (eq. 6 a) and the electrochemical desorption (Equation 6 b), respectively. The ratio of the experimentally determined currents $i_o^a / i_o^b \sim 0.1$, which agrees with this above mentioned assumption.

At $E \rightarrow 0$ one can obtain from Equation (7)

$$\left(\frac{\partial i}{\partial E}\right)_{E \rightarrow 0} = (F/RT) \cdot 4\, i_o^a \tag{10}$$

The value of i_o thus determined is about four times lower than that obtained experimentally (Table 1). As pointed out earlier (Fig. 5), at $E \rightarrow 0$, $\theta_H \sim 0.85$. In this case the overall reaction may include discharge (slow step) and recombination:

$$\begin{aligned} &H_2O + e^- \rightarrow H_{ads} + OH^- \quad \text{(slow)} \qquad (a) \\ &2\, H_{ads} \rightarrow H_2 \qquad (b) \end{aligned} \tag{11}$$

For reaction (11) the exchange current

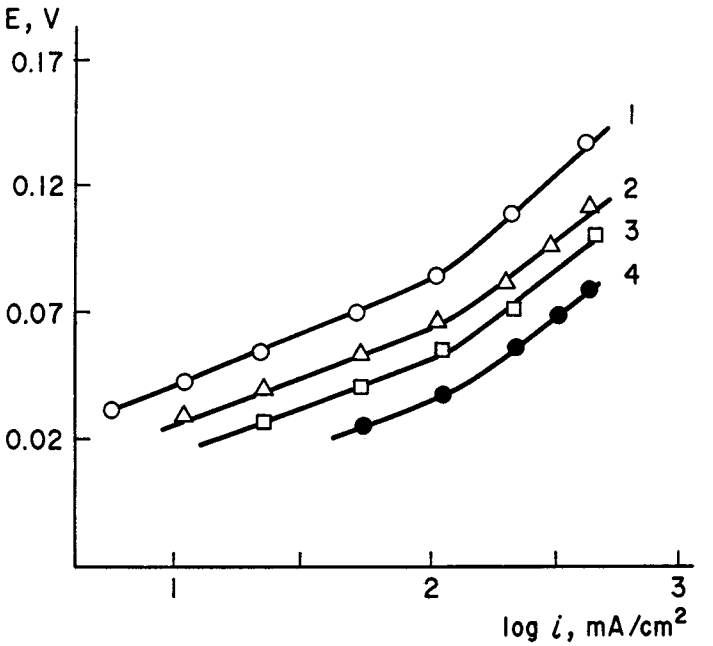

Fig. 9. Tafel plots, 7 N KOH, 70°C.
S_e, cm^2/cm^2: 1-2000, 2- 4000, 3- 5000, 4- 6000

$$i_0 = (RT/F)\left(\frac{\partial i}{\partial E}\right)_{E\to 0} \qquad (12)$$

according to the data of Table 1 $i_0 \approx i_0^a$.

The exchange currents given on Figs. 6, 7 were obtained on electrodes reduced at 600°C in hydrogen atmosphere. Immediately after leaching and removal into air the surface of the electrodes becomes air-oxidized. On such surface the exchange current is several times less than for reduced catalyst. Hydrogen reduction was carried out on air-oxidized catalyst. If catalyst was heated in hydrogen the exchange current in 0.1 N KOH at 25°C increased from 0.6 to 2.10^{-6} $A.cm^{-2}$.

Grid cathodes and anodes on the basis of a Ni-Co-P alloy with surface skeleton catalyst were tested in an electrolytic cell at 70°C and current density 0.4 $A.cm^{-2}$. The thickness of a porous asbestos separating matrix was 1.5 mm. The initial voltage was 1.85 V, the mean rate of voltage increase in 17,000 hours was 10 μV/hour.[8] The relative distribution of energy losses on the cathode $\left(\frac{\Delta E_c}{\Sigma \Delta E}\right)$, anode $\left(\frac{\Delta E_a}{\Sigma \Delta E}\right)$ and in the matrix $\left(\frac{\Delta E_m}{\Sigma \Delta E}\right)$, as well as the change in these losses in 10,000 hour operation is given in Table 2.

Special studies showed that deterioration of the cathode operation is to a large degree due to its poisoning by the leaching products of the separating matrix.

TABLE 2. Distribution of energy losses in the electrolytic cell $\Delta_m = 1.5$ mm, 7 N KOH, 70°C, $i = 0.4$ A. cm^{-2}

Parameter	$\tau = 0$ ΔE_j, %	$\tau = 10{,}000$ ΔE_j, %	Change of parameters in 10,000 hours
ΔE_c	22.2	30.7	44
ΔE_a	59.3	36.4	0
ΔE_m	18.5	32.2	56
$\Sigma \Delta E$	100	100	100

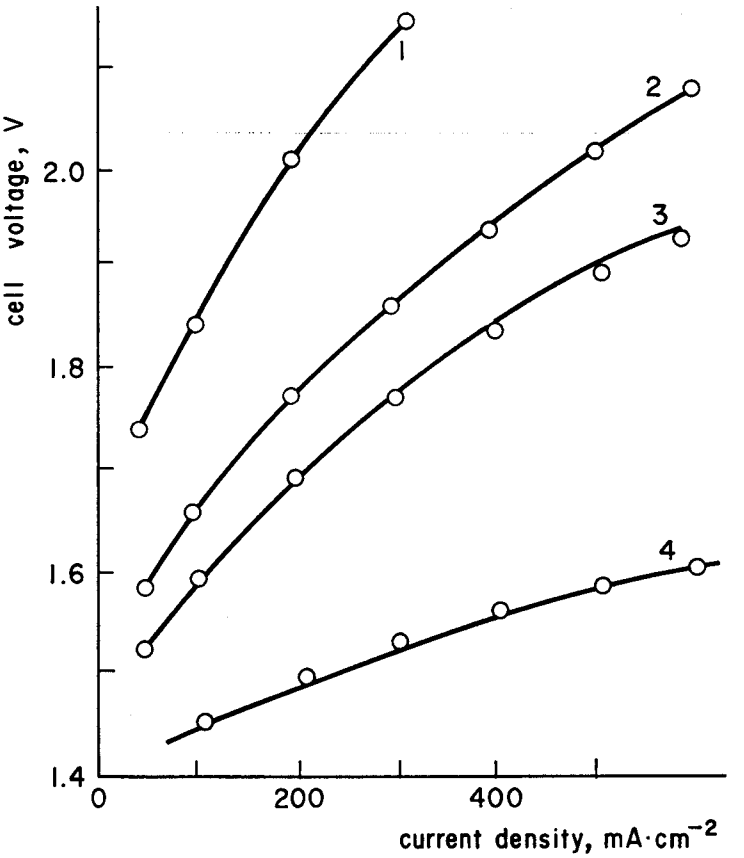

Fig. 10. Current voltage characteristics of electrolytic cells as a function of matrix thickness (Δ_m) and temperature (t°C), 7 N KOH.
Δ_m, mm: 1, 2, 3- 1.5, 4- 0.15 t°C: 1-22, 2- 70, 3, 4 -90

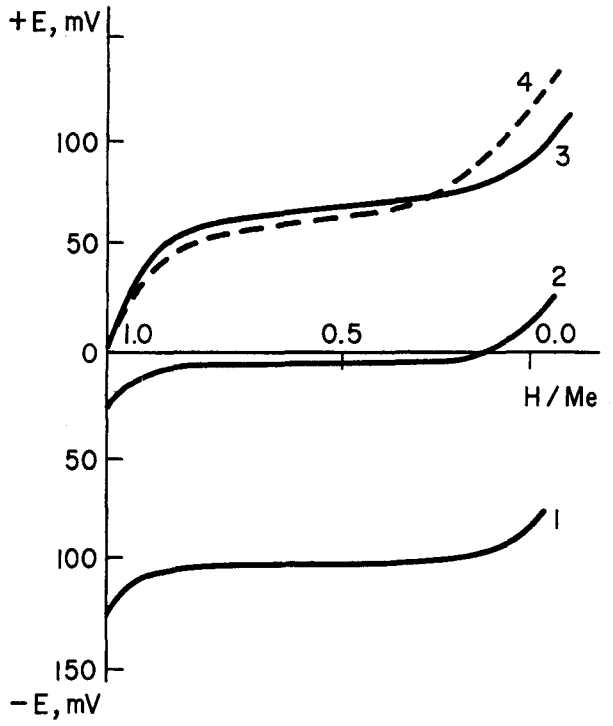

Fig. 11. Hydrogen absorption isotherms.
1–Ni, 2– alloy $LaNi_5$, 3–Pd, 4– alloy $LaNi_4Al$

The characteristics of electrolytic cells can be effectively improved by rising the working temperature to 90～95°C and decreasing the matrix thickness. Fig. 10 shows the current-voltage characteristics of electrolytic cells in the temperature range 25～90°C when matrixes 1.5 and 0.15 mm thick are used.

The properties of nickel as electrocatalyst of the hydrogen reaction can be drastically changed if alloys of nickel with other metals are used. Of particular interest are hydrogen absorbent alloys.[9] Thus the alloy $LaNi_5$ containing only 17 at.% La is a high-capacity hydrogen absorbent. Fig. 11 shows the hydrogen absorption isotherms plotted as potential versus hydrogen content for Ni,[10] Pd and the alloys $LaNi_5$ and $LaNi_4Al$. By varying the Al content in the alloy, it is possible to change in a wide range the pressure on the plateau (P_{H_2}). At $P<P_{H_2}$ hydrogen is desorbed from alloy. We found that in an electrochemical system the determining factor is not the partial hydrogen pressure but the total pressure in the system.[11] This phenomena can be explained by the scheme in Fig. 12. Under charge (cathodic polari-

zation) hydrogen can be removed from the system along the paths 1~3~6 and 1~4~5~6 by convection of gas bubbles and along the paths 1~4~7 by diffusion of molecular hydrogen. The overall rate of the diffusion path is much lower than that of the convection path due to the allowance of the diffusion processes in a porous electrode and solution bulk. We showed that as the first approximation hydrogen transfer along the diffusion path can be neglected. This reasoning is also valid for the self-discharge process (on Fig. 12 the path 2~3 (or 4~5~6). Since bubble formation is possible only at $P_{H_2} > P$, the self-discharge rate varies in agreement with the difference $P_{H_2} - P$ and the total pressure P can be produced by any gas. The equilibrium pressure P_{H_2} (and potential E_p) depends on temperature (Table 3).

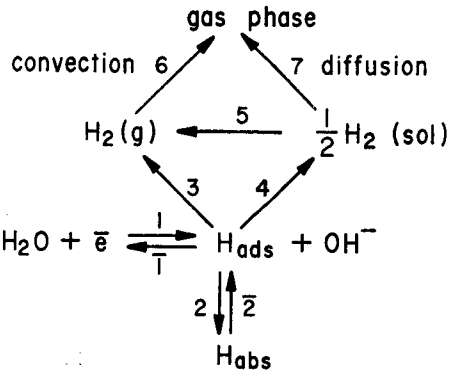

Fig. 12. Scheme of processes in the electrode system Ni_5LaH_x.

At P=const=1 atm the self-discharge rate increases with increasing temperature. At t=const (P_{H_2}=const) the self-discharge rate decreases with increasing total pressure. Fig. 13 shows the dependence of the self-discharge rate V_{sd} on P_A at 40°C. V_{sd} was determined by measuring the absorbed hydrogen amount (charge capacity of the electrode under standartized conditions) after electrode exposure at 40°C during 3 hours. At P=6 atm $V_{sd} \simeq 0$. When hydrogen was replaced by argon (gas over electrolyte in the electrolytic cell) the $V_{sd}(P)$ dependence does not change at all.

For investigation of the kinetics of the electrooxidation step of hydrogen dissolved in the alloy-hydrogen absorbent the reaction was carried out in the absence of diffusion-ohmic limitations in electrolyte.[12] The overall process at the catalyst grain/electrolyte interface includes two main steps:

TABLE 3. Equilibrium pressures on the plateau, P_{H_2}, as a function of temperature

t°C	−40	−20	0	20	40	60	80
P, atm	0.6	0.9	1.8	2.5	5.0	6.5	10
E, V	0.0064	0.0013	−0.0074	−0.011	−0.020	−0.024	−0.029

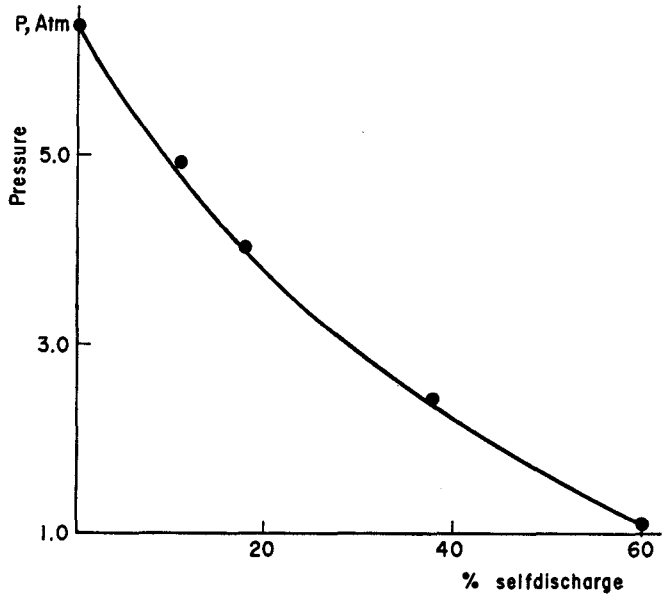

Fig. 13. Dependence of self-discharge of Ni_5LaH_x-electrode on inert gas pressure, 7 N KOH, 40°C.

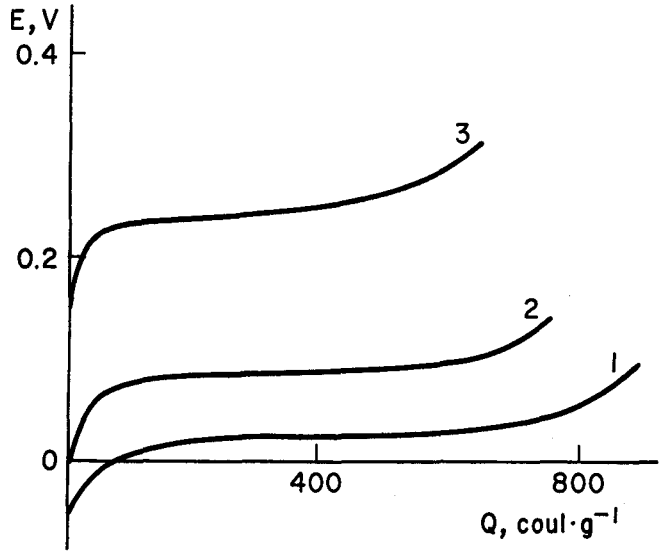

Fig. 14. Discharge curves of Ni_5LaH_6 electrodes at different current density, 7 NKOH, 20°C I, $mA \cdot cm^{-2}$: 1–30, 2–70, 3–150

$$H_{abs} \rightarrow H_{ads} \quad (a)$$
$$H_{abs} + OH^- \rightarrow H_2O + e \quad (b) \qquad (13)$$

In the general case the current density, i, at the catalyst grain electrolyte interface is a function of overpotential $E - E_{\theta_H}$, where E_{θ_H} is the equilibrium potential corresponding to the surface coverage by hydrogen Θ_H. Fig. 14 gives the discharge curves measured at different rates. The curves show the pressure of initial potential jump and independence of potential on hydrogen concentration in metal bulk. It is clear from the shape of the curves that Θ is constant when current densities up to 100 mA/cm^2 are used, *i. e.* the step (13 a) is fast and the electrochemical discharge step (13 b) is slow. From the dependence of the plateau potential on current density, knowing the surface of dispersed alloy (determined by BET) it is possible to calculate the exchange current of the reaction (13 b). The dependence of exchange current on temperature is given in Table 4.

TABLE 4. Dependence of the exchange current of the reaction (13 b) on temperature

t°C	−42	−20	−10	20	30	40	50	60
$i_0 10^6$ A·cm^{-2}	0.8	4.1	5.6	8.6	15	23	36	53

As pointed out earlier (see Fig. 7), the exchange current of the molecular hydrogen oxidation reaction on nickel in 7 N KOH at 20°C is $(1 \div 5).10^{-7}$ A.cm^{-2}. The exchange current of the reaction (13 b) is by an order of magnitude higher. This can be due both to slow rate of adsorption of molecular hydrogen on nickel and to electrocatalytic acceleration of the electrochemical step (13 b) on $LaNi_5$ alloy as compared with metallic nickel.

References

1) *Problems of electrocatalysis*, Nauka, Moscow, 1980, p. 271; Chapt. 3-6, p. 41-160.
2) L. A. Burkal'tseva and A. G. Pshenichnikov, Electrokhimiya, **12**, 42 (1976).
3) L. A. Burkal'tseva and A. G. Pshenichnikov, Elektrokhimiya, **13**, 248 (1977).
4) A. G. Pshenichnikov, R. H. Burshtein and V. D. Kovalevskaya, Elektrokhimiya, **11**, 1465 (1975).
5) A. G. Pshenichnikov, Z. I. Kudryavtseva, L. A. Burkal'tseva and N. A. Shumilova, Elektrokhimiya, **16**, 161 (1980).
6) A. G. Pshenichnikov, N. M. Savun and O. S. Abramson, Int. Soc. of Elektrochem. Power Sources, Varna, Bulg. Sept. 18-23, 1967, p. 272.

7) K. Vetter, *Elektrochemical kinetics*, M. Khimiya, 1967, p. 563.
8) A. G. Pshenichnikov, Hydrogen Energy, **1**, 51 (1982).
9) J. J. Reilly, *Metal hydrides as hydrogen storage media and their applications*, Hydrogen. Its techonology and Implecations, ed R. E. Cox, K. P. Williamson, 1977, No. 2, p. 142, p. 13–50.
10) B. Baranovskii, *Metal-hydrogen systems at high hydrogen pressures*, Hydrogen in Metals, Vol. 1, 1981, p. 209.
11) V. N. Zhuravleva, V. V. Karonik, A. G. Pshenichnikov and V. S., Bagotzky, Elektrohimiya, **16**, 1887 (1980).
12) V. N. Zhuravleva, A. G. Pshenichnikov, S. F. Chernyshov and B. I. T. Tsenter, Elektrokhimiya, **17**, 451 (1981).